© 2014. Published by The Company of Biologists Ltd | Journal of Cell Science (2014) 127, 281–287 doi:10.1242/jcs.140723

SHORT REPORT

# The conserved ciliary protein Bug22 controls planar beating of *Chlamydomonas* flagella

**Dan Meng[1,*], Muqing Cao[1,*], Toshiyuki Oda[2] and Junmin Pan[1,‡]**


## ABSTRACT

Eukaryotic flagella and cilia can exhibit planar and non-planar beating, and the mechanism controlling these beating patterns is not well understood. *Chlamydomonas reinhardtii* flagella beat in approximately the same plane with either an asymmetric ciliary-type or symmetric flagellar-type waveform. Each B-tubule of the number 1, 5 and 6 doublets of the flagellar axoneme possesses a beak-like structure. The number 5 and 6 beak structures are implicated in conversion of ciliary motion into flagellar motion. Here, we show that in a null mutant of *Bug22*, the asymmetric ciliary waveform is converted into a three-dimensional (non-planar) symmetric flagellar waveform. Bug22 is localized to approximately the proximal half to two-thirds of the flagellum, similar to localization of beak-like structures. However, as shown by immunogold labeling, Bug22 associates with axonemal microtubules without apparent preference for any particular doublets. Interestingly, *bug22* mutants lack all beak-like structures. We propose that one function of Bug22 is to regulate the anchoring of the beak-like structures to the doublet microtubules and confine flagellar beating to a plane.


**KEY WORDS: Bug22, *Chlamydomonas*, Cilia motility, Flagella, Cilia, Planar beating**

## INTRODUCTION

Motile cilia and eukaryotic flagella typically contain a '9+2' arrangement of axonemal microtubules attached with accessory structures, such as dynein arms and radial spokes, that are necessary for motility (Porter and Sale, 2000). In spite of this common structure, the beat patterns of cilia and flagella vary from a ciliary-type to a flagellar-type waveform. The ciliary waveform is a breaststroke-like asymmetric waveform with an effective stroke and a recovery stroke, and is exemplified by ciliary beating in protozoans such as *Paramecium* (Gibbons, 1981). The flagellar waveform is characterized by having a symmetric waveform, as observed during flagellar beating of spermatozoa (Gray, 1955; Gray, 1958).

As a model organism, *Chlamydomonas reinhardtii* is unique in that its flagella can alternate between ciliary and flagellar waveforms. Cells usually swim forwards, with flagella leading, by using ciliary strokes. In response to photoshock, cells swim backward, with flagella tailing, by using symmetric flagellar strokes (Ringo, 1967). The waveform switch depends on inherent structures of the axoneme. Structural studies have revealed the presence of beak-like structures within the B-tubule of the outer doublet microtubules (DMTs) 1, 5 and 6 along half to two-thirds of the proximal flagellum (Bui et al., 2009; Hoops and Witman, 1983). *mbo1* and *mbo2* mutants that lack beak-like structures in DMT 5 and 6 and display persistent flagellar strokes (Segal et al., 1984). The assembly of beak-like structures within DMT 5 and 6 requires *Mbo2*, which encodes an unknown conserved axonemal protein (Tam and Lefebvre, 2002). However, the function and regulation of the DMT 1 beak-like structure is unknown.

The beating of cilia and flagella can be planar or three-dimensional (non-planar) (Ginger et al., 2008). *Chlamydomonas* flagella beat in a planar manner during both ciliary and flagellar strokes (Ringo, 1967). However, the cilia of multiciliated protozoa such as *Paramecium* beat in three-dimensional patterns (Ginger et al., 2008). This indicates that the planar beating must be tightly controlled. In this work, we show that null mutant *bug22* loses all beak structures and that this is accompanied with the flagella beating becoming three-dimensional and having symmetric waveforms. This is in contrast to *mbo* mutants (Segal et al., 1984) and suggests that the DMT 1 beak might control planar beating of flagella.

## RESULTS AND DISCUSSION

### Flagellar motility mutant *2-20* loses control of planar beating and asymmetric waveforms

By using insertional mutagenesis with a DNA fragment harboring the paromomycin resistance *AphVIII* gene (Sizova et al., 2001), we obtained a flagellar motility mutant *2-20*. This mutant had two flagella of equal length (Fig. 1A). The mutant flagella were ~20% longer than wild type and displayed relatively sharp kinks (Fig. 1A,B), which might be formed by irregular bending of the flagella. When examining cell motility with low-speed video microscopy, wild-type cells showed swift directional movement (supplementary material Movie 1). In contrast, the mutant cells exhibited slow jerky movement with cells continuously turning around the body axis (supplementary material Movie 2). This non-directional movement was also reflected in a phototaxis assay. Unlike wild-type cells, *2-20* mutants failed to respond to illumination (Fig. 1C).

To determine the flagellar beating defect of the mutant, we examined the waveforms of flagella in *2-20* mutants by using dark-field high-speed video microscopy with wild-type cells as control. Flagella of wild-type cells beat in ciliary waveforms and in a planar manner (Fig. 1D; supplementary material Movie 3). In contrast, *bug22* flagella lost ciliary strokes and beat in flagellar waveforms in a three-dimensional non-planar fashion in a manner that was uncoordinated and severely deformed (Fig. 1D; supplementary material Movie 4).

[1]MOE Key Laboratory of Protein Science, School of Life Sciences, Tsinghua University, Beijing 100084, China. [2]Department of Cell Biology and Anatomy, Graduate School of Medicine, The University of Tokyo, Tokyo 113-0033, Japan.
*These authors contributed equally to this work

‡Author for correspondence (panjunmin@tsinghua.edu.cn)

**Received 14 August 2013; Accepted 30 October 2013**



Journal of Cell Science

Journal of Cell Science (2014) 127, 281–287 doi:10.1242/jcs.140723

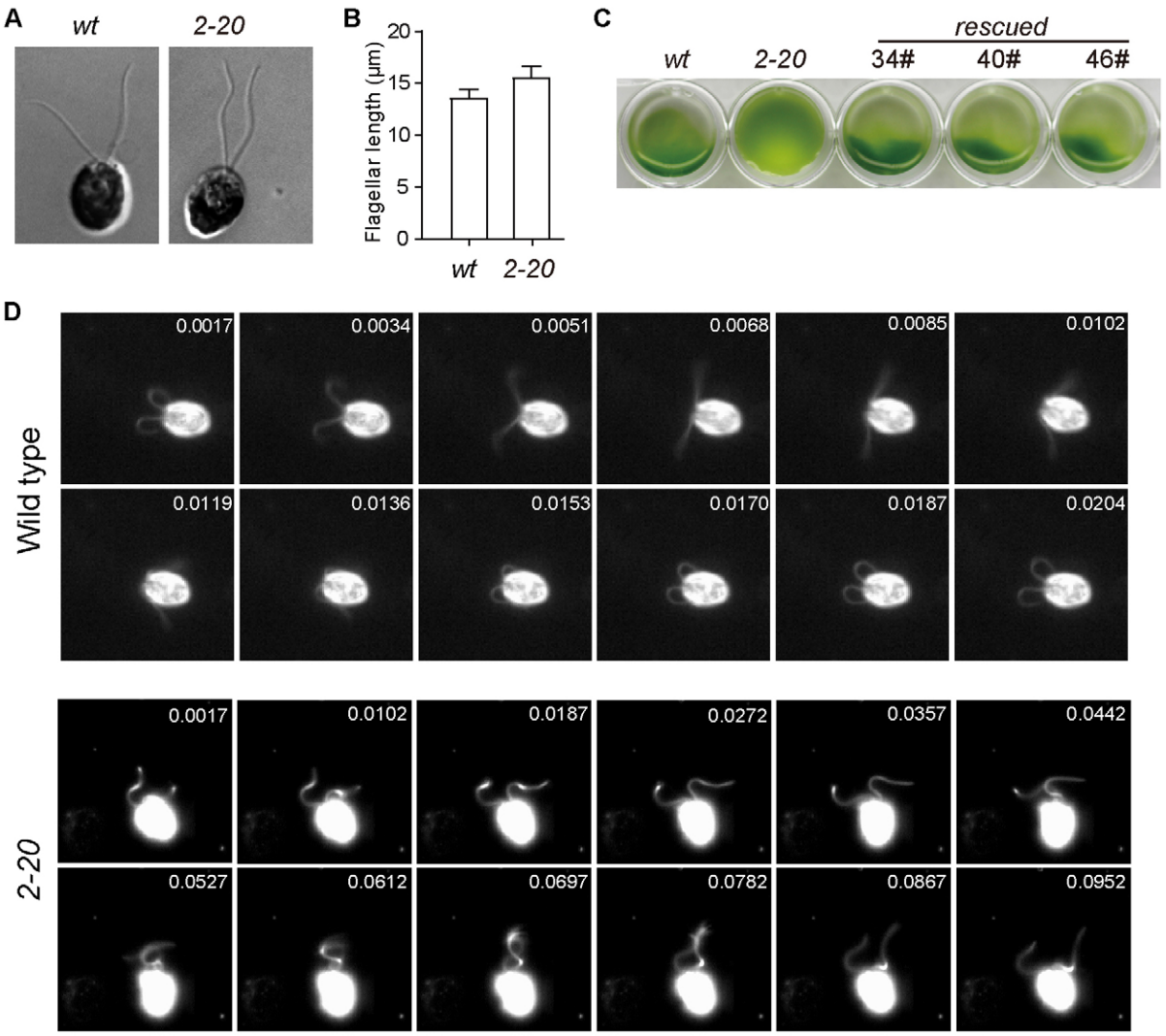


**Fig. 1. Mutant *2-20* loses planar flagellar beating and the asymmetric waveform.** (A) DIC images of a wild type (*wt*) and mutant *2-20* cell, showing the presence of two flagella with equal length and flagella with kinks in the mutant. (B) The gene mutation in *2-20* induces longer flagella. Cells from wild type (*wt*) and *2-20* were fixed in 1% glutaraldehyde and flagellar length from at least 50 cells was measured. Data are mean±s.d. $P<0.0001$. (C) The motility defect of *2-20* is reflected in phototaxis. A 24-well plate containing wild-type (*wt*), mutant *2-20* and rescued strains was illuminated on one side of the plate for 5 minutes followed by image capture. (D) Mutant *2-20* loses planar beating and the asymmetric waveform. Images of wild-type and mutant cells were taken at 600 frames per second. The time of each image is indicated. Note that wild-type flagella beat in planar manner in with asymmetric waveforms, which is defective in mutant *2-20*.

### Mutant *2-20* has defective *Bug22*

To identify the gene defective in mutant *2-20*, restriction enzyme site directed amplification (RESDA) PCR was used to clone the flanking sequence of the foreign DNA insert (González-Ballester et al., 2005). By searching the *Chlamydomonas* genome (http://genome.jgi-psf.org/Chlre4/Chlre4.home.html) with the flanking sequence, and subsequent DNA sequencing of the insertion region, the insert was localized to the second exon of the gene *Bug22* (also known as *FAP20*) and was accompanied by the loss of six nucleotides (Fig. 2A).

To determine whether disruption of *Bug22* was responsible for the phenotype observed, the *Bug22* gene tagged with triple hemagglutinin (*HA*) sequence was cloned into a plasmid containing the hygromycin resistance gene *aph 7″* followed by transformation into *bug22* mutants (Berthold et al., 2002). Three out of 100 transformants expressed Bug22–HA (Fig. 2B), and exhibited normal phototaxis and flagellar beating (Fig. 1C; supplementary material Movie 5). Although the flagellar beating frequency of *bug22* could not be measured because of severely deformed flagellar waveforms, the rescued strains showed similar beat frequency to that of wild type (72±10 Hz and 72±9 Hz in the wild-type and rescued strain, respectively). However, the rescued strain exhibited 18% less speed than wild type (148.9±6.3 versus 180.3±9.2 mm/second). The decreased speed in the rescued strain possibly resulted from a slightly winding swimming path (supplementary material Fig. S1), which is probably due to low expression of Bug22–HA (Fig. 2C). Immunoblotting analysis using a polyclonal antibody raised against two Bug22 synthetic peptides identified a band of around 22 kDa in wild type, which is similar to predicted molecular mass of Bug22 (Fig. 2C). In contrast, no similar band was detected in *bug22* mutants. The Bug22–HA protein expressed in the rescued

Journal of Cell Science (2014) 127, 281–287 doi:10.1242/jcs.140723

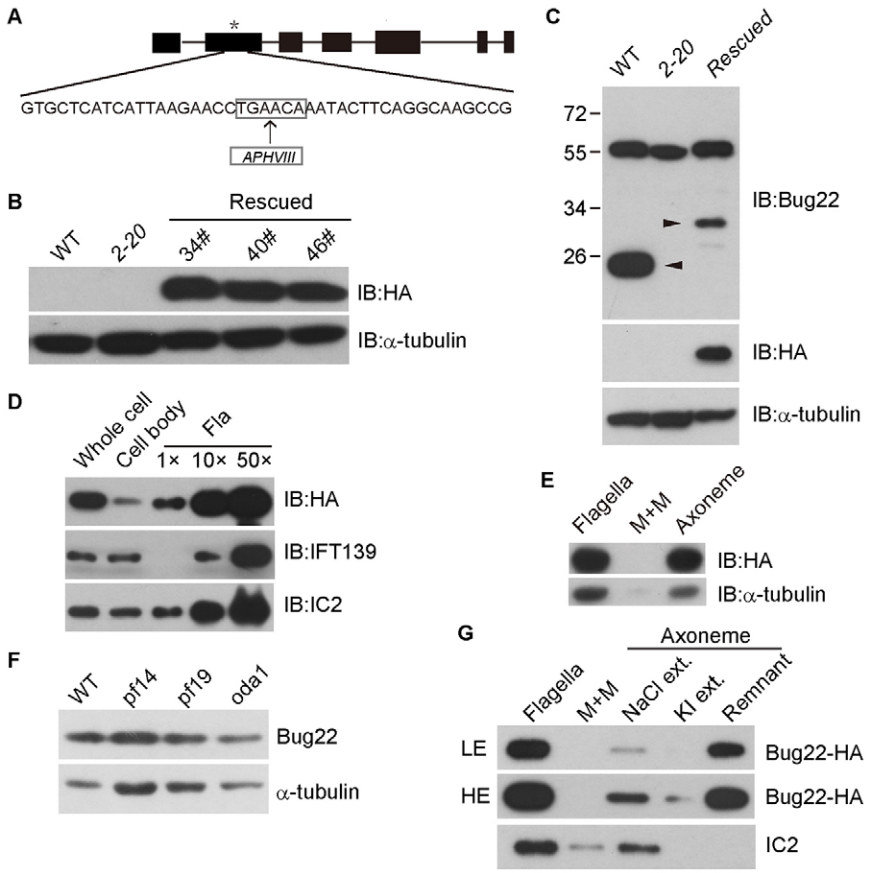


**Fig. 2. Mutant *2-20* is defective in *Bug22* whose protein product is tightly associated with axonemal microtubules.** (A) Schematic diagram of the *Bug22* gene showing the foreign DNA insertion in the second axon. The insertion site in the second exon (black box) is marked by an asterisk. The boxed six nucleotides were replaced by a DNA insert containing the *AphVIII* gene. The insertion site was identified by PCR and DNA sequencing. (B) Mutant *2-20* is rescued by expression of HA-tagged *Bug22*. Mutant *2-20* was transformed with HA-tagged *Bug22* and the transformants were analyzed by SDS-PAGE and immunoblotting with antibodies against HA and α-tubulin. Wild-type (WT) and mutant *2-20* were used as controls. (C) There is no protein expression of *Bug22* in mutant *2-20*. Cell lysates from the indicated strains were analyzed by SDS-PAGE and immunoblotting with antibodies against Bug22, HA and α-tubulin, respectively. Arrowheads indicate endogenous Bug22 or Bug22–HA. The molecular mass in kDa is shown on the left. (D) Bug22 is predominantly localized to the flagella. Cell body and flagella were isolated from cells expressing Bug22–HA followed by SDS-PAGE and immunoblotting with anti-HA antibody. 1×fla (flagella) represents an equal proportion of flagella to that of the cell body. Antibodies against IFT proteins (IFT139) and dynein arm protein (IC2) were used as controls. (E) Bug22 is an axonemal protein. Isolated flagella of the rescued strain expressing Bug22–HA was fractionated into a membrane matrix fraction (M+M) and axoneme by using 0.5% NP-40. 5 μg of flagella and an equal proportion of the flagellar fractions were subjected to immunoblot analysis with the indicated antibodies. (F) Immunoblot analysis of flagella isolated from mutants lacking various axonemal structures. *pf14* is deficient in radial spoke, *pf19* central pair, and *oda1* outer dynein arms. (G) Bug22 is tightly associated with axonemal microtubules. Flagella were first fractionated into membrane matrix and axonemal fractions. The axoneme was further extracted with 0.6 M NaCl followed by extraction with 0.2 M KI. 2 μg of flagella and equal proportions of fractions were analyzed by SDS-PAGE and immunoblotting with the antibodies indicated. LE and HE represent results from low and high exposures of the same blot, respectively.

strain was also recognized by this antibody. Thus, *Bug22* is the defective gene in *2-20* and its mutation is responsible for the mutant phenotype. The mutant *2-20* was thus named *bug22*.

### Bug22 is an abundant axonemal protein and tightly associates with the axonemal microtubules

Bug22 has previously been identified both in the basal body proteome (Keller et al., 2005) and the flagellar proteome of *Chlamydomonas* (Pazour et al., 2005). This protein is highly conserved in ciliated organisms as well as in higher plants (Hodges et al., 2011; Laligné et al., 2010). Alignment of Bug22 with its human ortholog (GenBank NP_037374.1) showed 89% identity within 98% coverage. Bug22 has been shown to be a flagellar protein in *Paramecium* and *Trypanosome* (Hodges et al., 2011; Laligné et al., 2010). Immunogold labeling of Bug22 in *Paramecium* shows that it is preferentially localized between ciliary membrane and axoneme, as well as to basal bodies. Knockdown of *Bug22* expression by RNAi in this organism results in the conversion of the ciliary waveform to the flagellar waveform, which is consistent with our results (Laligné et al., 2010).

To confirm whether Bug22 is a flagellar protein in *Chlamydomonas*, Bug22–HA-expressing cells were fractionated into cell body and flagellar fractions and subjected to immunoblot analysis. Compared with intraflagellar transport (IFT) proteins, represented by IFT139 and the outer dynein arm protein IC2 (previously known as IC69) (Hom et al., 2011), Bug22 was even more enriched in the flagella (Fig. 2D). Flagellar fractionation followed by SDS-PAGE and immunoblot analysis showed that Bug22 was exclusively localized to the axonemal fraction (Fig. 2E). SDS-PAGE analysis of the mutant flagella followed by Coomassie Blue staining revealed that *bug22* mutants were

Journal of Cell Science (2014) 127, 281–287 doi:10.1242/jcs.140723

deficient in a 22 kDa protein, which was identified as Bug22 by mass spectrometry analysis, indicating that Bug22 is an abundant axonemal protein (supplementary material Fig. S2).

To determine whether Bug22 associated with any particular axonemal structures, we analyzed flagella of various flagellar mutants by immunoblotting (Fig. 2F). Bug22 appeared to be normal in the flagella of mutants missing radial spokes (*pf14*) (Piperno et al., 1977), central pair microtubules (*pf19*) (Dymek and Smith, 2012) and outer dynein arms (*oda1*) (Kamiya and Okamoto, 1985). To refine the localization of Bug22 in the axoneme, the flagellar axoneme was further fractionated by using 0.6 M NaCl followed by 0.2 M potassium iodide (KI) extraction. It has been reported that high-salt extraction solubilizes outer dynein arms, partial inner dynein arms and the C2 microtubule of the central pair but leaves outer DMTs and radial spokes intact, and that further extraction with KI removes the C1 microtubule (Mitchell and Sale, 1999; Piperno and Luck, 1979). Immunoblot analysis of these fractions showed that the majority of Bug22 was resistant to high-salt and KI extraction (Fig. 2G). This fractionation assay along with analysis of flagellar mutants indicates that most of Bug22 is associated with outer DMTs with only a minor amount associated with the central pair microtubules.

#### All beak projections in B-tubules are missing in the *bug22* mutant

Backward swimming mutants *mbo1* and *mbo2* lose both beak projections in DMT 5 and 6 but not in DMT 1 and convert ciliary waveforms into flagellar waveforms (Segal et al., 1984; Tam and Lefebvre, 2002). One of the motility phenotypes of *bug22* included loss of ciliary waveforms, indicating that the beak-like structures might be also defective in *bug22*. The beak-like structures are present in the proximal half to two-thirds of the flagellum (Hoops and Witman, 1983; Pigino et al., 2012). Thus, we first examined Bug22 distribution in the flagellum by immunostaining using an anti-HA antibody (Fig. 3A). As expected, no HA staining was observed in *bug22* mutants. In the *bug22* mutants rescued by expression of Bug22–HA we found polarized staining in the proximal half to two-thirds of the flagellum. This staining pattern is coincident with the distribution of the beak-like structures.

Next, we examined possible flagellar structural defects of *bug22* using electron microscopy. The orientation of the two basal bodies was similar in wild type and mutant cells (Fig. 3B,C), which was however altered in Bug22 RNAi strains of *Paramecium* (Laligné et al., 2010). In addition, the 'H' structure and Y-links in the transition zone appeared normal in the mutant compared with wild type (Fig. 3D,E). Cross-sections of the axoneme revealed the presence of outer doublet and central pair microtubules, and dynein arms in both mutant and wild type (Fig. 3F,G). As expected, we noticed that the beak-like structures in the B-tubules of DMT 5 and 6 were missing in the mutant, but 1–2 bridge was present. Surprisingly, the beak projection in DMT 1 was also missing. These data are distinct from the loss of beak-like structures in *mbo* mutants (Segal et al., 1984), and indicate that Bug22 is a common regulator affecting all beak-like structures.

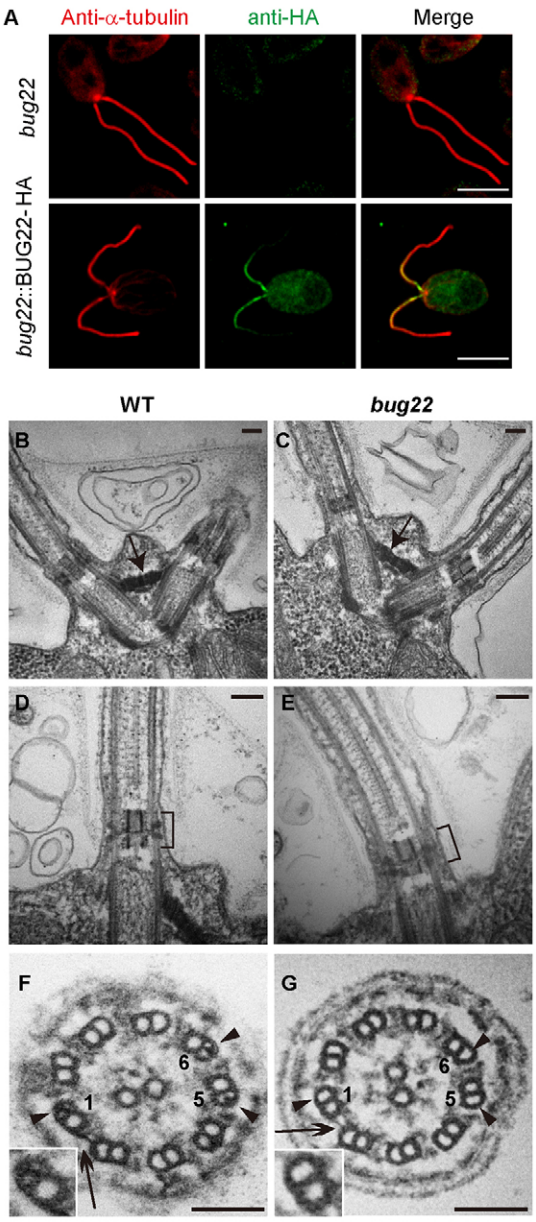


**Fig. 3. Bug22 mutation results in loss of beak structures within the B-tubule of outer doublet 1, 5 and 6.** (A) Bug22 is localized to the proximal half to two-thirds of the flagella. *bug22* and the rescued strain expressing Bug22–HA were immunostained with antibodies against HA and α-tubulin. Note HA staining was not detected in the mutant, but predominantly localized to the proximal half to two-thirds of flagella in the rescued strain. (B,C) Longitudinal sections through the basal bodies show no difference between wild-type (WT) and *bug22* in the orientation of the two basal bodies connected by the distal striated fiber (arrow). (D,E) Normal appearance of the 'H'-shaped structure and Y-links in the transition zone region (brackets) in the mutant and wild type. (F,G) Flagellar cross sections show the presence of the 1–2 bridges (arrows) between DMT 1 and 2 in both wild-type and *bug22* strains, and the beak-like structures (arrowheads) of the wild-type flagella within the B-tubule of DMT1, 5 and 6, which were missing in *bug22*. Insets are enlarged images of DMT 1. Scale bars: 5 μm (A), 100 nm (B–G).

#### Bug22 associates with all axonemal microtubules

To determine whether Bug22 is specifically localized to DMT 1, 5 and 6, we examined the localization of Bug22 in the axoneme by immunogold labeling. Using anti-HA antibody and cells that were rescued with the HA-tagged *Bug22* gene, we observed that the gold particles labeled the transition zone, the basal body and the axoneme (Fig. 4A,B). Most of the particles were close to or on the axonemal microtubules in longitudinal sections. In cross sections, the gold particles concentrated on or close to outer doublet and central pair microtubules (Fig. 4C; supplementary

Journal of Cell Science (2014) 127, 281–287 doi:10.1242/jcs.140723

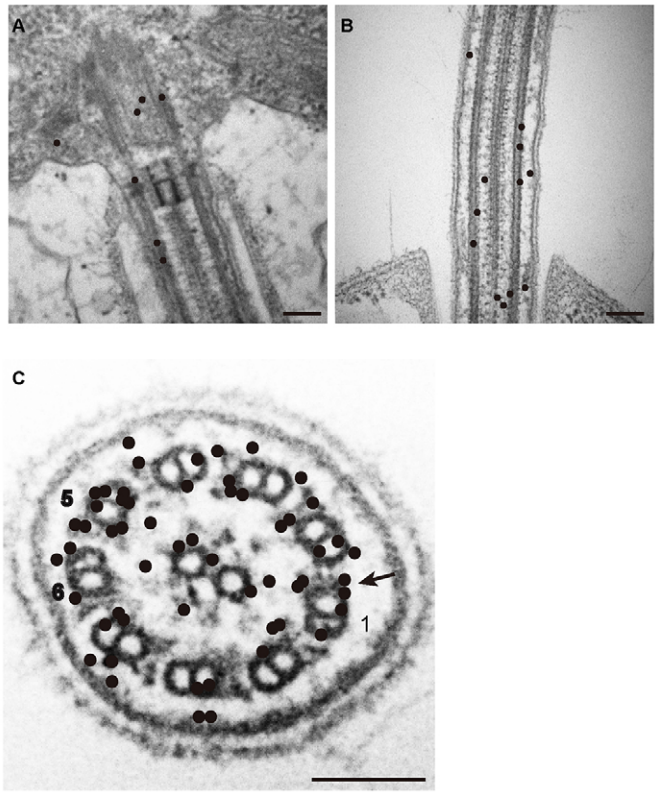


**Fig. 4. Immunogold localization of Bug22.** (A–C) Cells expressing Bug22–HA were fixed, embedded and sectioned followed by incubation with anti-HA antibody and gold-conjugated secondary antibody (12-nm gold). Gold particles were observed in the basal body (A) and along axonemal microtubules (B). In cross section, the locations of particles from 30 sections are depicted by black dots superimposed on a single electron microscopy image (C). A selection of original micrographs is shown in supplementary material Fig. S3. Scale bars: 100 nm.

material Fig. S3). Interestingly, there was no preferred localization of particles surrounding DMT 1, 5 and 6. Under the same experimental conditions, rare labeling was observed in the flagella of wild-type cells by using anti-HA antibody (supplementary material Fig. S3).

The loss of beak structures in DMT 5 and 6 in *mbo* mutants results in the conversion of asymmetric waveforms to symmetric waveforms (Segal et al., 1984). Similar waveform conversion in *bug22* is probably due to, at least in part, the loss of the two beak-like structures. Flagella of *mbo1* and *mbo2* mutants are both deficient in six common polypeptides, accompanying loss of the two beak structures, indicating these two beak structures might be identical (Segal et al., 1984). We propose that Bug22 is not a component of the beak-like structures and serves as a microtubule-binding protein in order to regulate their anchoring. First, Bug22 is not one of the proteins deficient in the flagella of *mbo* mutants. Second, the null mutant *bug22* loses all beak-like structures.

The association of Bug22 with all axonemal microtubules indicates that it has an additional function to anchoring of the beak-like structures. The deformed flagellar waveforms of the mutant might reflect the loss of flagellar rigidity. The abundant presence of Bug22 in the axoneme and its tight association with axonemal microtubules might provide stability and stiffness to the axoneme. It has been shown that the proximal half to two-thirds of the flagellum is more stable and resistant to drug-induced flagellar shortening (Dentler and Adams, 1992). It has also been proposed that Bug22 in *Paramecium* might regulate cilia rigidity (Laligné et al., 2010). It is interesting that Bug22 appears to be much more abundant than outer row dynein subunits of similar size. It is unknown how it is arranged in the axoneme.

*Chlamydomonas* can swim forwards and backwards with distinct waveforms, but the flagella always beat in a planar manner regardless of the waveform (Ringo, 1967). *bug22* lost control of planar beating with the flagellar beating in three dimensions. Planar beating in *mbo* mutants is not affected after loss of the two beak-like structures (Segal et al., 1984). Hence, the beak-like structure within B-tubule of DMT 1 is probably responsible for planar beating. Cryo-electron tomography has revealed that the beak-like structure is 3-nm thick and has a 6-nm-wide band running along the inside of B-tubule perpendicular to the flagellar beating plane (Nicastro et al., 2011). This structure is analogous to a jigsaw blade that allows only two-dimensional bending. The multiciliated organisms, such as *Paramecium* and possibly *Tetrahymena*, have cilia that beat in three-dimensional ciliary waveforms (Gibbons, 1981; Ginger et al., 2008). The flagella of sea urchin can switch between planar beating and a helical three-dimensional waveform depending on the viscosity of the medium (Woolley and Vernon, 2001). Interestingly, cryo-electron tomography analysis of cilia of *Tetrahymena* and flagella of sea urchin fails to identify similar structures (Pigino et al., 2012). Thus, the beak structure in DMT 1 might be specifically used by *Chlamydomonas* to control planar beating.

## MATERIALS AND METHODS

### Strains and cell culture

Cell culture in liquid and on agar plates were described elsewhere (Wang et al., 2013). Briefly, vegetative cells grown in liquid M medium were cultured at 23℃ with aeration under 14:10 hour light-dark cycle. The following *Chlamydomonas reinhardtii* strains were used: *21gr* (mt+) (CC-1690), *oda1* (mt−) (CC-2229), *pf19* (mt+) (CC-1037) and *pf14* (mt−) (CC-613), which are available from the *Chlamydomonas* Genetics Center, University of Minnesota.

### Insertional mutagenesis, gene cloning and transformation

To generate insertional mutants, the wild-type strain *21gr* was transformed with the 2.1 kb *APHVIII* fragment from plasmid pIS103m, a derivative of pIS103 (Sizova et al., 2001). RESDA PCR was used to identify the genomic sequences flanking the *APHVIII* insertion site of the mutant (González-Ballester et al., 2005). The insertion site was further identified by PCR and sequencing.

To generate a construct for expressing *Bug22* with a 3×HA tag at its 3′-end in *Chlamydomonas*, the *Bug22* gene, with an approximately 1 kb fragment upstream of its start codon, was cloned by PCR and a 3×HA tag sequence with a Rubisco terminator was cloned from plasmid pKL-3xHA (kindly provided by Karl F. Lechtreck, University of Georgia, Athens, GA) (Lechtreck et al., 2009). Then tagged gene was cloned into a modified vector pHyg3 harboring a Hygromycine B resistance gene (Berthold et al., 2002). The final construct was linearized with *Sca*I and transformed into the *bug22* mutant by using electroporation (Liang and Pan, 2013).

### Cell fractionation, flagellar length measurements and DIC cell images

The cell body and flagella were isolated after deflagellation by pH shock (Wang et al., 2013). After deflagellation and purification, the cell bodies were dissolved in HMDEK buffer (50 mM Tris-HCl pH 7.5, 10 mM $MgCl_2$, 1 mM EDTA, 1 mM DTT, 25 mM KCl) containing 0.5% NP40 and complete protease inhibitor cocktail (Roche), and flash frozen in liquid nitrogen. The flagella were further purified by sucrose gradient centrifugation and the purified flagella were dissolved in the buffer

described above and frozen in liquid nitrogen. For flagellar fractionation, the flagella were first thawed on ice and centrifuged at 30,000 ***g*** for 10 minutes at 4℃ (Eppendorf 5417R). The supernatant was collected as the membrane matrix fraction. The pelleted axonemal fraction was either collected directly or further extracted with 0.6 M NaCl followed by 0.2 M KI, following a published protocol (Mitchell and Sale, 1999). Flagellar length measurement and capture of DIC images were essentially as described previously (Liang and Pan, 2013).

### SDS-PAGE and immunoblotting

Analysis for SDS-PAGE and immunoblotting was essentially as described previously (Liang and Pan, 2013). Cells were collected by centrifugation and lysed with HMDEK buffer containing an EDTA-free protease inhibitor cocktail (Roche) prior to boiling in SDS-PAGE sample buffer. Antibodies used were: mouse anti-α-tubulin (1:2500 for whole cells or 1:100,000 for flagella, Sigma), rat anti-HA (1:4000, Roche), mouse anti-IFT139 (1:10,000), mouse anti-IFT81 (1:1000), mouse anti-IC69 (1:20,000, Sigma) and rabbit anti-Bug22 (1:5000). IFT antibodies were kindly provided by Douglas Cole (University of Idaho, Moscow, ID). The anti-Bug22 antibody was made by injecting two peptides [EIWDKQVSNGHIKRITDC (amino acids 23–39), CEEELPAEFK-LFLPIQKS (amino acids 174–190)] into rabbits and affinity purified.

### Immunofluorescence Microscopy

Immunostaining analysis was preformed essentially as described previously (Wang et al., 2013). The primary antibodies used were: rat monoclonal anti-HA (1:50, clone 3F10, Roche), mouse monoclonal anti-α-tubulin (1:200, Sigma). The secondary antibodies used were Texas-Red-conjugated goat anti-mouse IgG (1:400, Molecular Probes) and Alexa-Fluor-488-conjugated goat anti-rabbit IgG (1:400, Molecular Probes). The samples were viewed on a Zeiss LSM780 META Observer Z1 Confocal Laser Microscope. Images were acquired and processed by ZEN 2009 Light Edition (Zeiss) and Adobe Photoshop software (Adobe).

### Electron microscopy and immunogold labeling

For electron microscopy, a published method was followed with the following modifications (Craige et al., 2010). After removal of primary fixative by centrifugation, the cells were gently resuspended in 20 ml buffer A (0.5%NP40, 50 mM sodium cacodylate and 0.6M NaCl, pH 7.2) for 20 minutes at room temperature followed by fixation with secondary fixative. Sections were imaged on a transmission electron microscope (H-7650B; Hitachi Limited). Images were acquired using a digital AMT V600 camera (ATM Company).

For immuno-EM, the sections were prepared as described above except without treatment with buffer A after primary fixation and 0.1% instead of 1% $OsO_4$ was used for post-fixation. The primary and secondary antibodies used were rat monoclonal anti-HA (1:50, clone 3F10, Roche) and 12-nm-gold-conjugated goat anti-rat IgG (1:20, Jackson ImmunoResearch), respectively. Samples were imaged on an electron microscope (H-7650B; Hitachi Limited). Images were acquired using a digital camera (ATM Company).

### Analysis by mass spectrometry

A total of 25 µg flagellar proteins from wild-type and *bug22* cells were analyzed by SDS-PAGE followed by Coomassie Blue staining. The 22 kDa protein band missing from the mutant flagellar axoneme was exercised and subjected to protein determination by mass spectrometry in the protein core facility at Tsinghua university (Wang et al., 2013).

### Cell motility and waveform analysis

For the phototaxis dish assay, cells were placed in 24-well microtiter plates and illuminated on one side of the plate. Images were taken 5 minutes after illumination by using a Nikon D90 digital camera (Nikon, Japan). Low speed video was recorded using DIC optics in Zeiss Axo Observer with a 40× objective (Zeiss, Germany) equipped with a QuantumEM 512SC camera (Photometrics, USA). The images were captured at 12.7 fps for wild type and 11.3 fps for the mutant. High-speed video microscopy was performed using a dark-field microscope (BX51, Olympus) equipped with a Mikrotron MC1362 camera (Mikrotron, Germany). The images were taken at 600 fps. Phase-contrast optics and a 50× objective were used. For the swimming path assay, the cells were observed using a 10× objective lens under an IX70 microscope (Olympus) and captured at 30 fps with a progressive scan type camera (MC681 SPD, Texas Instruments). The tracking images of the swimming path were processed with the ImageJ plugin 'Particle Tracker' (NIH) (Sbalzarini and Koumoutsakos, 2005).

### Acknowledgements

We are grateful to Ying Li for excellent help with the electron microscopy analysis and to Masahide Kikkawa (University of Tokyo) for the valuable discussions and suggestions.

### Competing interests

The authors declare that they have no conflict of interest.

### Author contributions

M.D., M.C. and T.O. performed experiments. M.D., M.C., T.O. and J.P. designed the study. M.D., M.C. and J.P. wrote the paper.

### Funding

This work was supported by the 973 program [grant numbers 2012CB945003, 2013CB910700 to J.P.]; and the National Natural Science Foundation of China [grant numbers 30830057, 30988004 to J.P.].

### Supplementary material

Supplementary material available online at
http://jcs.biologists.org/lookup/suppl/doi:10.1242/jcs.140723/-/DC1

### References

**Berthold, P., Schmitt, R. and Mages, W.** (2002). An engineered Streptomyces hygroscopicus aph 7″ gene mediates dominant resistance against hygromycin B in Chlamydomonas reinhardtii. *Protist* **153**, 401-412.
**Bui, K. H., Sakakibara, H., Movassagh, T., Oiwa, K. and Ishikawa, T.** (2009). Asymmetry of inner dynein arms and inter-doublet links in Chlamydomonas flagella. *J. Cell Biol.* **186**, 437-446.
**Craige, B., Tsao, C. C., Diener, D. R., Hou, Y., Lechtreck, K. F., Rosenbaum, J. L. and Witman, G. B.** (2010). CEP290 tethers flagellar transition zone microtubules to the membrane and regulates flagellar protein content. *J. Cell Biol.* **190**, 927-940.
**Dentler, W. L. and Adams, C.** (1992). Flagellar microtubule dynamics in Chlamydomonas: cytochalasin D induces periods of microtubule shortening and elongation; and colchicine induces disassembly of the distal, but not proximal, half of the flagellum. *J. Cell Biol.* **117**, 1289-1298.
**Dymek, E. E. and Smith, E. F.** (2012). PF19 encodes the p60 catalytic subunit of katanin and is required for assembly of the flagellar central apparatus in Chlamydomonas. *J. Cell Sci.* **125**, 3357-3366.
**Gibbons, I. R.** (1981). Cilia and flagella of eukaryotes. *J. Cell Biol.* **91**, 107s-124s.
**Ginger, M. L., Portman, N. and McKean, P. G.** (2008). Swimming with protists: perception, motility and flagellum assembly. *Nat. Rev. Microbiol.* **6**, 838-850.
**González-Ballester, D., de Montaigu, A., Galván, A. and Fernández, E.** (2005). Restriction enzyme site-directed amplification PCR: a tool to identify regions flanking a marker DNA. *Anal. Biochem.* **340**, 330-335.
**Gray, J.** (1955). The movement of sea-urchin spermatozoa. *J. Exp. Biol.* **32**, 775-801.
**Gray, J.** (1958). The movement of the spermatozoa of the bull. *J. Exp. Biol.* **35**, 96-108.
**Hodges, M. E., Wickstead, B., Gull, K. and Langdale, J. A.** (2011). Conservation of ciliary proteins in plants with no cilia. *BMC Plant Biol.* **11**, 185.
**Hom, E. F., Witman, G. B., Harris, E. H., Dutcher, S. K., Kamiya, R., Mitchell, D. R., Pazour, G. J., Porter, M. E., Sale, W. S., Wirschell, M. et al.** (2011). A unified taxonomy for ciliary dyneins. *Cytoskeleton (Hoboken)* **68**, 555-565.
**Hoops, H. J. and Witman, G. B.** (1983). Outer doublet heterogeneity reveals structural polarity related to beat direction in Chlamydomonas flagella. *J. Cell Biol.* **97**, 902-908.
**Kamiya, R. and Okamoto, M.** (1985). A mutant of Chlamydomonas reinhardtii that lacks the flagellar outer dynein arm but can swim. *J. Cell Sci.* **74**, 181-191.
**Keller, L. C., Romijn, E. P., Zamora, I., Yates, J. R., 3rd and Marshall, W. F.** (2005). Proteomic analysis of isolated chlamydomonas centrioles reveals orthologs of ciliary-disease genes. *Curr. Biol.* **15**, 1090-1098.
**Laligné, C., Klotz, C., de Loubresse, N. G., Lemullois, M., Hori, M., Laurent, F. X., Papon, J. F., Louis, B., Cohen, J. and Koll, F.** (2010). Bug22p, a conserved centrosomal/ciliary protein also present in higher plants, is required for an effective ciliary stroke in Paramecium. *Eukaryot. Cell* **9**, 645-655.
**Lechtreck, K. F., Luro, S., Awata, J. and Witman, G. B.** (2009). HA-tagging of putative flagellar proteins in Chlamydomonas reinhardtii identifies a novel

protein of intraflagellar transport complex B. *Cell Motil. Cytoskeleton* **66**, 469-482.
**Liang, Y. and Pan, J.** (2013). Regulation of flagellar biogenesis by a calcium dependent protein kinase in Chlamydomonas reinhardtii. *PLoS ONE* **8**, e69902.
**Mitchell, D. R. and Sale, W. S.** (1999). Characterization of a Chlamydomonas insertional mutant that disrupts flagellar central pair microtubule-associated structures. *J. Cell Biol.* **144**, 293-304.
**Nicastro, D., Fu, X., Heuser, T., Tso, A., Porter, M. E. and Linck, R. W.** (2011). Cryo-electron tomography reveals conserved features of doublet microtubules in flagella. *Proc. Natl. Acad. Sci. USA* **108**, E845-E853.
**Pazour, G. J., Agrin, N., Leszyk, J. and Witman, G. B.** (2005). Proteomic analysis of a eukaryotic cilium. *J. Cell Biol.* **170**, 103-113.
**Pigino, G., Maheshwari, A., Bui, K. H., Shingyoji, C., Kamimura, S. and Ishikawa, T.** (2012). Comparative structural analysis of eukaryotic flagella and cilia from Chlamydomonas, Tetrahymena, and sea urchins. *J. Struct. Biol.* **178**, 199-206.
**Piperno, G. and Luck, D. J.** (1979). Axonemal adenosine triphosphatases from flagella of Chlamydomonas reinhardtii. Purification of two dyneins. *J. Biol. Chem*. **254**, 3084-3090.
**Piperno, G., Huang, B. and Luck, D. J.** (1977). Two-dimensional analysis of flagellar proteins from wild-type and paralyzed mutants of Chlamydomonas reinhardtii. *Proc. Natl. Acad. Sci. USA* **74**, 1600-1604.
**Porter, M. E. and Sale, W. S.** (2000). The 9 + 2 axoneme anchors multiple inner arm dyneins and a network of kinases and phosphatases that control motility. *J. Cell Biol.* **151**, F37-F42.
**Ringo, D. L.** (1967). Flagellar motion and fine structure of the flagellar apparatus in Chlamydomonas. *J. Cell Biol.* **33**, 543-571.
**Sbalzarini, I. F. and Koumoutsakos, P.** (2005). Feature point tracking and trajectory analysis for video imaging in cell biology. *J. Struct. Biol.* **151**, 182-195.
**Segal, R. A., Huang, B., Ramanis, Z. and Luck, D. J.** (1984). Mutant strains of Chlamydomonas reinhardtii that move backwards only. *J. Cell Biol.* **98**, 2026-2034.
**Sizova, I., Fuhrmann, M. and Hegemann, P.** (2001). A Streptomyces rimosus aphVIII gene coding for a new type phosphotransferase provides stable antibiotic resistance to Chlamydomonas reinhardtii. *Gene* **277**, 221-229.
**Tam, L. W. and Lefebvre, P. A.** (2002). The Chlamydomonas MBO2 locus encodes a conserved coiled-coil protein important for flagellar waveform conversion. *Cell Motil. Cytoskeleton* **51**, 197-212.
**Wang, L., Piao, T., Cao, M., Qin, T., Huang, L., Deng, H., Mao, T. and Pan, J.** (2013). Flagellar regeneration requires cytoplasmic microtubule depolymerization and kinesin-13. *J. Cell Sci.* **126**, 1531-1540.
**Woolley, D. M. and Vernon, G. G.** (2001). A study of helical and planar waves on sea urchin sperm flagella, with a theory of how they are generated. *J. Exp. Biol.* **204**, 1333-1345.